



1 **Regional and global climate response to anthropogenic**
2 **SO₂ emissions from China in three climate models**

3

4 **M. Kasoar¹, A. Voulgarakis¹, J.-F. Lamarque², D. T. Shindell³, N. Bellouin⁴, W. J.**
5 **Collins⁴, G. Faluvegi⁵, and K. Tsigaridis⁵**

6 [1]{Department of Physics, Imperial College London, London, UK}

7 [2]{NCAR Earth System Laboratory, National Center for Atmospheric Research, Boulder,
8 CO, USA}

9 [3]{Nicholas School of the Environment, Duke University, Durham, NC, USA}

10 [4]{Department of Meteorology, University of Reading, Reading, UK}

11 [5]{Center for Climate Systems Research, Columbia University, and NASA Goddard Institute
12 for Space Studies, New York, NY, USA}

13 Correspondence to: M. Kasoar (m.kasoar12@imperial.ac.uk)

14

15 **Abstract**

16 We use the HadGEM3-GA4, CESM1, and GISS ModelE2 climate models to investigate the
17 global and regional aerosol burden, radiative flux, and surface temperature responses to
18 removing anthropogenic sulfur dioxide (SO₂) emissions from China. We find that the models
19 differ by up to a factor of six in the simulated change in aerosol optical depth (AOD) and
20 shortwave radiative flux over China that results from reduced sulfate aerosol, leading to a
21 large range of magnitudes in the regional and global temperature responses. Two of the three
22 models simulate a near-ubiquitous hemispheric warming due to the regional SO₂ removal,
23 with similarities in the local and remote pattern of response, but overall with a substantially
24 different magnitude. The third model simulates almost no significant temperature response.
25 We attribute the discrepancies in the response to a combination of substantial differences in
26 the chemical conversion of SO₂ to sulfate, translation of sulfate mass into AOD, and
27 differences in the radiative forcing efficiency of sulfate aerosol in the models. The model
28 with the strongest response (HadGEM3-GA4) compares best with observations of AOD



1 regionally, however the other two models compare similarly (albeit poorly) and still disagree
2 substantially in their simulated climate response, indicating that total AOD observations are
3 far from sufficient to determine which model response is more plausible. Our results
4 highlight that there remains a large uncertainty in the representation of both aerosol chemistry
5 as well as direct and indirect aerosol radiative effects in current climate models, and
6 reinforces that caution must be applied when interpreting the results of single-model studies
7 of aerosol influences on climate. Model studies that implicate aerosols in climate responses
8 should ideally explore a range of radiative forcing strengths representative of this uncertainty,
9 in addition to thoroughly evaluating the models used against observations.

10

11 **1 Introduction**

12 Short-lived atmospheric pollutants such as aerosols have very inhomogeneous spatial
13 distributions. This means that, unlike long-lived greenhouse gases such as CO₂, the radiative
14 forcing due to aerosols is highly variable, and the resulting climate response may be strongly
15 influenced by the region of emission and the prevailing circulation patterns. There is
16 increasing interest in trying to understand how aerosol forcing from different regions affects
17 the climate, both locally and remotely. For example, Shindell and Faluvegi (2009) and
18 Shindell et al. (2012) looked systematically at the response of temperature and precipitation to
19 single-species forcings imposed in different latitude bands, and showed that the influence of
20 remote forcings on certain regions can often outweigh and even have opposite sign to the
21 influence of local forcings. Teng et al. (2012) investigated the global temperature response to
22 drastically increasing carbonaceous aerosols only over Asia, finding a strong remote effect on
23 US summertime temperatures.

24 One of the most important anthropogenically-sourced aerosol species is sulfate (SO₄) (e.g.
25 Myhre et al., 2013b). Sulfate-containing aerosols are formed following chemical conversion
26 of gaseous sulfur dioxide (SO₂) emissions from fossil-fuel combustion, as well as natural
27 sources such as volcanic SO₂ and ocean dimethyl sulfide (DMS) emissions (e.g. Andres and
28 Kasgnoc, 1998; Andreae and Crutzen, 1997). Sulfate particles strongly scatter incoming
29 shortwave (SW) radiation, which helps to increase the planetary albedo and cool the surface.
30 They also act as cloud condensation nuclei, leading to additional cloud droplets forming in
31 supersaturated conditions, which increases cloud albedo and again cools the Earth system.



1 Historically, cooling from sulfate aerosol, predominantly in the more industrialised northern
2 hemisphere, has been implicated by a range of modelling studies in disrupting climate since
3 the mid-20th century. For instance Booth et al. (2012), Hwang et al. (2013), and Wilcox et al.
4 (2013) discussed the importance of historical aerosol cooling in modulating large-scale
5 temperature and precipitation patterns, while other studies such as Bollasina et al. (2011),
6 Dong et al. (2014), and Polson et al. (2014) have looked at the impact of historical aerosols on
7 regional climate features such as the monsoon systems or Sahelian rainfall.

8 The few studies that have investigated specific regional aerosol forcings (e.g. Shindell and
9 Faluvegi (2009); Shindell et al. (2012); Teng et al. (2012)) typically used a single climate
10 model at a time to investigate the climate response to idealised, historical, or projected
11 forcings. However models vary considerably in their representation of aerosols and their
12 radiative properties, resulting in a large uncertainty in aerosol radiative forcing (e.g. Myhre et
13 al., 2013b; Shindell et al., 2013a). When investigating the climate response to regional
14 aerosol emissions, such uncertainties are likely to be confounded even further by the
15 variability between models in regional climate and circulation patterns, and variation in the
16 global and regional climate sensitivity (the amount of simulated warming per unit radiative
17 forcing). To best interpret the findings of single-model experiments with regional aerosol
18 forcings, it is therefore critical to understand the range of uncertainty in the climate response
19 that may arise as a result of structural and parametric differences between climate models.

20 We investigate here the range of variability that can arise in the translation of a regional
21 emission perturbation to a climate (temperature) response, between three different state-of-
22 the-art global climate models. We select as a case study the removal of SO₂ anthropogenic
23 emissions from the region of China. Since China is currently the largest anthropogenic source
24 region of sulfur dioxide (Smith et al., 2011) and hence anthropogenic aerosol, this regional
25 perturbation represents a substantial modification to global aerosol levels, with the additional
26 characteristic of being localised over a particular part of the world. This aspect of our
27 experiment is distinct from many previous model intercomparison studies, which have
28 typically compared the climate response in models forced by global historical trends in
29 aerosols (for example, Shindell et al., 2015; Wilcox et al., 2013), or which have only
30 considered the impact of regional emissions on long-range pollution transport and on radiative
31 forcing (for example the HTAP and AeroCom experiments (HTAP, 2010; Yu et al., 2013;
32 Kinne et al., 2006; Schulz et al., 2006; Textor et al., 2006)), but have not investigated the



1 range of model climate responses to a regionally localised emission perturbation. The
2 potential importance of remote climate effects due to the strong zonal asymmetry created by
3 such regional emissions has therefore not yet been explored in multi-model studies. Single-
4 model studies such as Teng et al. (2012) suggest though that regionally localised forcings can
5 produce significant climate teleconnections in at least the longitudinal direction.

6 In the following sections we first describe the three models employed, and our experimental
7 setup (Sect. 2). We then present the results of the radiative flux and surface temperature
8 responses to the removal of Chinese SO₂ (Sect. 3), and analyse the possible reasons for
9 differences between the model responses (Sect. 4). Finally, in Sect. 5 we present our
10 conclusions.

11

12 **2 Model descriptions and experimental set-up**

13 The three models we employ are the Hadley Centre Global Environment Model 3 – Global
14 Atmosphere 4.0 (HadGEM3-GA4), the Community Earth System Model 1 (CESM1), and the
15 Goddard Institute for Space Studies ModelE2 (GISS-E2). To allow the climate system to
16 freely respond, the models are all used in a fully coupled atmosphere-ocean configuration.
17 These three models all feature explicit aerosol modelling, and include both direct and indirect
18 radiative effects of aerosols. However the models all vary in the details of the
19 parameterisations used, the dynamical cores, radiation and cloud schemes, model grids and
20 horizontal and vertical resolutions, land surface and ocean components, etc. This lack of
21 common structural features make these three models well suited to contrast against one
22 another and probe the range of potential model uncertainty, as we do here.

23

24 **2.1 Model descriptions**

25 **2.1.1 HadGEM3-GA4**

26 For HadGEM3, we use the Global Atmosphere 4.0 version of the model in a standard climate
27 configuration with a horizontal resolution of 1.875° longitude x 1.25° latitude in the
28 atmosphere, with 85 vertical levels and the model top at 85km, dynamically resolving the
29 stratosphere. The atmosphere is coupled to the JULES land surface model, which includes 4
30 soil layers and 5 plant functional types. Although in principle this can be run in a fully



1 interactive ‘Earth-System’ mode with dynamic vegetation and a carbon cycle, here we
2 prescribe fixed vegetation and also prescribe globally-uniform observed mass-mixing ratios
3 for CO₂, CH₄, and other long-lived greenhouse gases, taking their year-2000 values from the
4 CMIP5 historical dataset. A zonally-uniform present-day ozone climatology is also
5 prescribed in the radiation scheme, derived from the SPARC dataset (Cionni et al., 2011).
6 More detailed description and evaluation of the atmosphere and land-surface schemes can be
7 found in Walters et al. (2014). The atmospheric model is also coupled to the NEMO
8 dynamical ocean model (Madec, 2008) and CICE sea-ice model (Hunke and Lipscombe,
9 2008), which are run with a 1° horizontal resolution, and 75 vertical depth levels for the
10 ocean.

11 Critical to our study is the representation of aerosols; we use the CLASSIC aerosol scheme,
12 which is described and evaluated in Bellouin et al. (2011). CLASSIC is a mass-based scheme
13 which includes an interactive representation of sulfate in three modes (Aitken, accumulation,
14 and in-cloud), fossil-fuel black carbon, fossil-fuel organic carbon, and biomass-burning
15 aerosol in three modes (fresh, aged, and in-cloud), dust in six size bins, and sea-salt in two
16 modes (jet and film), as well as an offline biogenic aerosol climatology. The scheme can also
17 include a representation of nitrate aerosol, but this option was not used here.

18 The sulfate component of the scheme (Jones et al., 2001) includes tracers for two gas-phase
19 precursors: SO₂ from anthropogenic and natural sources, and DMS from natural sources.
20 These are emitted into the atmosphere and can undergo advection, wet and dry deposition, or
21 oxidation using prescribed 4D oxidant fields (Derwent et al., 2003). In CLASSIC, oxidation
22 of SO₂ to SO₄ aerosol can proceed through three possible reaction pathways: in the gas phase
23 by reaction with OH, or in the aqueous phase by reaction with either H₂O₂ or O₃.

24 The remaining aerosol species are emitted directly in the particulate phase, and all aerosol
25 species can then undergo advection, wet and dry deposition, and interaction with radiation.
26 The hygroscopic aerosols (sulfate, organic carbon, biomass-burning aerosol, sea-salt) can also
27 interact with clouds via their role as cloud condensation nuclei. Cloud droplet number
28 concentration and effective radius are determined from the concentration of these aerosols,
29 which affects the simulated cloud lifetime (2nd indirect effect) and cloud brightness (1st
30 indirect effect) as described in Bellouin et al. (2011) and Jones et al. (2001).

31



1 **2.1.2 CESM1**

2 CESM1 is run in its standard CAM5-Chem configuration (Tilmes et al., 2015) with a
3 horizontal resolution of 2.5° longitude x 1.875° latitude, and 30 vertical levels, with the model
4 top at approximately 40 km. The atmosphere is coupled to the Community Land Atmosphere
5 version 4 land surface model (Lawrence et al., 2011). In the present configuration, the
6 vegetation distribution is fixed at its 2005 distribution and the CO₂ concentration is specified.
7 The atmosphere model is coupled to the POP2 ocean and CICE4 sea-ice models, with an
8 equivalent resolution of 1°.

9 In the present CAM5-Chem configuration (Tilmes et al., 2015), we use a representation of
10 tropospheric and stratospheric chemistry so that no chemical constituents are specified, other
11 than specifying the long-lived greenhouse gases' concentrations in the surface layer. The gas-
12 phase chemistry is coupled to the modal aerosol scheme MAM3 (Liu et al., 2012), so that the
13 rate of formation of sulfate aerosols is dependent on the chemical state of the atmosphere.
14 SO₂ from anthropogenic and natural sources can be converted to SO₄ through three oxidation
15 pathways: by OH in the gas phase, or by either H₂O₂ or O₃ in the aqueous phase. In addition,
16 the surface area of the prognostic tropospheric aerosols is used to compute heterogeneous
17 reaction rates that affect gas-phase chemistry. Aerosols interact with climate through radiation
18 and cloud-aerosol interactions.

19

20 **2.1.3 GISS-E2**

21 GISS-E2 is run in the configuration used for CMIP5 with a horizontal resolution of 2.5°
22 longitude x 2° latitude, and 40 vertical levels, with the model top at 0.1 hPa (80 km). The
23 atmospheric model is coupled to the dynamic Russell ocean model with horizontal resolution
24 of 1° latitude x 1.25° longitude, and 32 vertical levels as described in Schmidt et al. (2013)
25 and Russell et al. (1995).

26 Well-mixed greenhouse gases are prescribed as described in Miller et al. (2013), but methane
27 is only prescribed at the surface and is otherwise interactive with the chemistry. The ozone
28 distribution is prognostic throughout the simulated atmosphere, and the chemical mechanism
29 is described in Shindell et al. (2013b). In general, other atmospheric gas and aerosol
30 constituents are also simulated online and interact with each other (via oxidants in both the
31 gas and aqueous phases, heterogeneous chemistry, aerosol-influenced gas photolysis, and



1 aerosol-coating of dust) and with climate (via radiative effects of ozone and methane, water
2 vapour change due to chemistry, and aerosol direct and indirect effects) in a manner
3 consistent with the physics of the rest of the GCM as described in Sect. 3b of Schmidt et al.
4 (2013). For the sulfur scheme in particular, SO₂ from anthropogenic and natural sources can
5 be oxidised to SO₄ aerosol through two reaction pathways: by OH in the gas phase, or by
6 H₂O₂ in the aqueous phase.

7 Other aerosols include nitrate, elemental and organic carbon (Koch et al. 2011; 2006) along
8 with secondary organic aerosols and natural sea-salt and mineral dust. Aerosol indirect effects
9 are calculated as described in Menon et al. (2010).

10

11 **2.2 Experimental setup**

12 For this study we investigate the surface temperature response to an idealised regional
13 emission perturbation, on a centennial timescale. Each model has a control simulation which
14 is forced with the same anthropogenic emissions of aerosols and their precursors following
15 the year-2000 ACCMIP emission inventory (Lamarque et al., 2010). The control simulations
16 are run for 200 years with continuous year-2000 conditions. For each model, we then run a
17 200-year perturbation simulation in which SO₂ emissions from energy production, industry,
18 transport, domestic use, and waste, are set to zero over the region of China, defined here to be
19 the rectangular domain 80°-120°E, 20°-50°N. These emission sectors contribute 98.7% of the
20 anthropogenic SO₂ emitted from this region, so this corresponds to a near complete removal
21 of SO₂ emissions from this highly polluting area of the globe. Quantitatively, this
22 perturbation reduces global anthropogenic SO₂ emissions from around 104 Tg yr⁻¹ to 86 Tg
23 yr⁻¹, a reduction of around 17 Tg yr⁻¹, or 16.5%.

24

25 **3 Radiative forcing and climate response**

26 We investigate the change in the mean state of the models by taking averages over the last
27 150 years of the 200-year-long simulations (the first 50 years were discarded as spin-up), and
28 taking the difference between the perturbation simulation and the control simulation. As well
29 as plotting maps of 2D variables, we also calculate area-weighted means of temperature,
30 short-wave radiative flux, and aerosol optical depth, both globally and for an east China



1 region (E. China) defined as 100°-120°E, 20°-40°N. This region is found to contain the most
2 intense changes in sulfate aerosol in all three models, and is used from here on to quantify the
3 magnitude of local changes over China. The global- and regionally-averaged quantities are
4 tabulated in Table 1, along with the total sulfate burdens over the globe and E. China, and the
5 ratios of AOD to sulfate burden and SW flux to AOD changes.

6 The anticipated immediate consequence of removing SO₂ emissions from China is that there
7 will be a reduction in the amount of sulfate aerosol formed, leading to a positive shortwave
8 (SW) radiative forcing. Figure 1 shows the changes in net downward top-of-atmosphere
9 (TOA) SW radiative flux in each of the three models. For HadGEM3-GA4 and GISS-E2, the
10 plot is stippled in locations where the change exceeds two standard deviations, estimated for
11 HadGEM3-GA4 from the grid-point standard deviations from six year-2000 control runs with
12 perturbed atmospheric initial conditions, and for GISS-E2 from 12 non-overlapping 150-year
13 sections of a 1900-year-long pre-industrial control simulation that had reached radiative
14 equilibrium.

15 Figure 1 reveals that there is a very substantial variation between the models in the intensity
16 of the local radiative flux change over China. GISS-E2 shows a fairly weak increase in net
17 downward SW flux over E. China, with a local increase (from Table 1) of 0.91 W m⁻² and an
18 insignificant global mean change (-0.034 W m⁻²), whereas HadGEM3-GA4 shows a very
19 pronounced change of 5.3 W m⁻² locally over E. China, and a global mean value of 0.28 W m⁻².
20 CESM1 lies in the middle, with a moderate local SW flux change of 4.2 W m⁻², and 0.19
21 W m⁻² in the global mean. Between GISS-E2 and HadGEM3-GA4, there is a 6-fold increase
22 in the intensity of the local radiative flux change over E. China.

23 Because these are fully coupled simulations, the change in the TOA SW flux does not provide
24 a measure of the shortwave radiative forcing, since the underlying climate has been allowed to
25 adjust, potentially allowing feedbacks on clouds, and snow and ice cover. A complementary
26 pair of atmosphere-only simulations, where sea-surface temperatures (SSTs) and sea-ice cover
27 were prescribed to year-2000 values, were run with HadGEM3-GA4 to diagnose the effective
28 radiative forcing (ERF) – the change in TOA radiative flux when feedbacks due to the slow
29 response of the ocean are prevented (Andrews et al., 2010). The global SW ERF due to
30 removing SO₂ from China in these fixed-SST simulations is 0.18 W m⁻², 35% smaller than
31 the 0.28 W m⁻² change in the fully coupled case. However, locally over the E. China region,
32 the fixed-SST change was found to be 4.2 W m⁻², which is only 21% lower than the 5.3 W m⁻²



1 value in the fully coupled experiment. Moreover, the spatial map of the SW flux anomaly
2 over China is very similar between the two experiments (Supplementary fig. S1). At least in
3 HadGEM3-GA4, over E. China the change in sulfate therefore appears to be the dominant
4 driver of the change in TOA SW flux, and the local change in SW flux over this region is
5 reasonably representative of the local radiative effect of the sulfate perturbation even in the
6 fully-coupled simulations with this model. The same is less true of the global-mean values
7 because of positive feedback from ice melt in the Arctic, and also some small but widespread
8 changes in cloud cover, which globally add up to a sizeable effect in the coupled simulations
9 (not shown).

10 Based on the fully coupled simulations, the substantial differences in the intensity of SW flux
11 changes over China ultimately translate to very pronounced differences in the strength of the
12 resulting climate response. Figure 2 shows the change in surface air temperatures between
13 the perturbation and control runs for each of the three models. Again stippling indicates the
14 response exceeds the 2σ level in HadGEM3-GA4 and GISS-E2. The difference between
15 GISS-E2 and HadGEM3-GA4 is particularly striking. Apart from a small warming in parts of
16 eastern China by around 0.1 K, there is virtually no coherent temperature response across the
17 rest of the globe in GISS-E2. The global mean temperature change (Table 1) is -0.028 K and
18 is not significant. In contrast HadGEM3-GA4 displays significant warming across almost all
19 of the northern hemisphere, with much larger increases in temperature between 0.4-1 K in
20 many regions, not only in China but also in much of the US, northern Eurasia, and the Arctic.
21 The global mean temperature response is +0.11 K. CESM1 sits again in the middle, with
22 clear warming responses between 0.2-0.5 K over much of eastern Europe, Asia, and the west
23 Pacific. Overall the warming response is still less strong and less widespread than in
24 HadGEM3-GA4, with a global mean warming of +0.054 K.

25 The spatial pattern of warming over Europe and Asia in CESM1 bears some qualitative
26 similarity though to the pattern over the same region in HadGEM3-GA4, suggesting that there
27 may be a similar mode of global response to heating over eastern China in these models, at
28 least across the Eurasian continent. The dynamical mechanisms through which local aerosol
29 emissions are translated to remote response are beyond the scope of this manuscript though.
30 Whether GISS-E2 would have displayed the same pattern had the radiative forcing over
31 China been stronger is impossible to tell from these results; given the small magnitude of the
32 SW flux change it seems that most of the spatial pattern in the temperature response in GISS-



1 E2 can be attributed to internal variability – the largest changes in temperature seen in this
2 model are in fact a region of cooling over the north-west Atlantic, which is mostly not
3 significant and appears instead to be the result of particularly large internal variability in this
4 region.

5

6 **4 Exploring drivers of diversity**

7 We investigate the differences between these models that lead to such a large variation in the
8 predicted temperature response. We explore below a number of possible sources of
9 discrepancy.

10

11 **4.1 Differences in simulated aerosol amounts**

12 We address first the possibility that differences in the aerosol schemes themselves, lead
13 directly to very different aerosol loadings between the models, despite the identical change in
14 SO₂ emissions applied. Figure 3 shows the change in column-integrated SO₄ in each model
15 as a result of removing Chinese SO₂ emissions. The models vary in both the distribution and
16 magnitude of SO₄ reductions. In particular, HadGEM3-GA4 has the reduction in SO₄ burden
17 fairly concentrated over China. CESM1 and GISS-E2 simulate more diffuse changes in SO₄
18 which extend further downwind from the source region, giving a larger spatial footprint. This
19 difference in spatial extent of the SO₄ field from Chinese SO₂ seems to be due to particularly
20 fast conversion of SO₂ to SO₄ in HadGEM3-GA4 resulting in much more concentrated
21 changes in SO₄ close to the source. For GISS-E2 and HadGEM3-GA4 where more detailed
22 diagnostics were available, we find that the SO₂ lifetime is around 1.8 times shorter in
23 HadGEM3-GA4, associated with around 45% higher wet oxidation rates in this model. This
24 difference is due in part to the inclusion of an additional wet oxidation pathway in
25 HadGEM3-GA4: whereas GISS-E2 only includes wet oxidation of SO₂ by H₂O₂ (around 730
26 kg(S) s⁻¹ globally integrated), HadGEM3-GA4 includes wet oxidation by both H₂O₂ and O₃,
27 each of which contribute similarly in this model (around 540 kg(S) s⁻¹ and 520 kg(S) s⁻¹
28 respectively).

29 Globally integrated, HadGEM3-GA4 and GISS-E2 simulate fairly similar reductions in SO₄
30 burden, at -0.070 Tg and -0.077 Tg respectively (Table 1). This, combined with the more



1 spread-out SO₄ field in GISS-E2, means that locally over eastern China HadGEM3-GA4 has a
2 much more intense reduction in SO₄ burden, with 50% of the global reduction occurring over
3 E. China in HadGEM3-GA4 (-0.035 Tg), compared with only 21% (-0.016 Tg) in GISS-E2.
4 CESM1, by contrast, simulates almost double the global change in SO₄ burden as the other
5 two models, with -0.136 Tg. This means that although the SO₄ reduction spreads further from
6 the source in CESM1 than in HadGEM3-GA4, CESM1 still has a similar reduction to
7 HadGEM3-GA4 locally over E. China (-0.039 Tg).

8 Given that HadGEM3-GA4 and GISS-E2 simulate a similar global reduction in SO₄, it is
9 surprising that there is such a difference in the magnitude of their climate responses. Also,
10 given that CESM1 simulates a much larger global reduction in SO₄ than the other two models,
11 it is similarly surprising that this model does not have the largest response. A partial
12 explanation may be found by inspecting the change in total aerosol optical depth (AOD),
13 which is a more direct measure of the radiative properties of the aerosol column.
14 Unfortunately, the AOD diagnosed by the models is not completely equivalent: HadGEM3-
15 GA4 diagnosed clear-sky AOD, which is done in this model by calculating the relative
16 humidity in the cloud-free portion of each grid-box, and using this adjusted humidity to
17 calculate the size of the aerosol droplets in the optical depth calculation (Bellouin et al.,
18 2007). However CESM1 uses the unadjusted grid-box relative humidity to calculate the
19 droplet sizes in its optical depth calculation, thereby providing an all-sky AOD calculation
20 (Neale et al., 2012). GISS-E2 diagnosed both all-sky and clear-sky AOD, and unless
21 otherwise stated we compare here its clear-sky AOD, as it is more directly comparable with
22 satellite retrievals of AOD (Kahn et al., 2010; Levy et al., 2013). Figure 4 shows these
23 changes in AOD at the 550nm wavelength for the three models.

24 As with the radiative flux change, there is a large range in the magnitude of local AOD
25 reduction, with E. China AOD reductions ranging from 0.047 in GISS-E2 to 0.287 in
26 HadGEM3-GA4, i.e. about 6 times higher (Table 1). This is comparable to the approximately
27 6-fold range of SW flux change found over this region. Globally averaged, HadGEM3-GA4
28 also has a much larger AOD reduction than GISS-E2; 0.0042 compared with an almost
29 negligible 0.0003 in GISS-E2, despite these two models having a similar change in global
30 SO₄ burden. The much lower globally-averaged value in GISS is partly due to a very small
31 but quite zonally-uniform compensating increase in nitrate aerosol, (absent in HadGEM3-
32 GA4), which occurs across the northern hemisphere (not shown). However, the global



1 change in sulfate-only optical depth in GISS-E2 is still only half that in HadGEM3-GA4 (not
2 shown), and locally around eastern China we find the increase in nitrate optical depth in
3 GISS-E2 is at least an order of magnitude smaller than the decrease in sulfate optical depth,
4 and so nitrate compensation does not substantially contribute to the discrepancy in local AOD
5 changes. We therefore still find that HadGEM3-GA4 simulates a considerably larger change
6 in sulfate optical depth per unit change in SO₄ burden at both global and local scales. Having
7 the largest change in AOD per unit change in aerosol burden (Table 1) appears to be key to
8 this model simulating the largest climate response.

9 Comparing the clear-sky and all-sky AOD for GISS-E2 (for which we have both diagnostics),
10 we find that the simulated reduction in all-sky AOD (-0.183) is much larger than the reduction
11 in clear-sky AOD (-0.047). We cannot be sure that the same would apply to CESM1, but it
12 suggests that we might expect the all-sky values we have for CESM1 to be larger than the
13 equivalent clear-sky values. Given this, it is surprising to find reductions of all-sky AOD in
14 CESM1 for the E. China region of -0.076 and for the global mean of -0.0013 (Table 1), which
15 lie in between the clear-sky values of GISS-E2 and HadGEM3-GA4 even though CESM1 had
16 the largest change in SO₄ burden both locally and globally.

17 The change in SW radiative flux and the final climate response seem to correlate with the
18 change in AOD much better than with the change in SO₄ burden for HadGEM3-GA4 and
19 GISS-E2, where over China there is a 6-fold difference both in AOD and in SW flux change
20 between these two models. For CESM1, the all-sky AOD changes over E. China are about
21 1.6 times larger than the clear-sky changes in GISS-E2 (Table 1). If we used instead all-sky
22 AOD from GISS-E2 (not shown in Table 1), we find that the AOD change over E. China is
23 more than 2 times smaller in CESM1 than in GISS-E2. However, the change in TOA SW
24 over the same region is about 4.7 times larger in CESM1, and so it seems that unlike the
25 discrepancies between HadGEM3-GA4 and GISS-E2, differences in the AOD response
26 cannot explain the difference in the magnitudes of radiative flux change between CESM1 and
27 GISS-E2 (see Sect. 4.3).

28

29 **4.1.1 Validation of aerosol fields**

30 To get an indication of whether the model-simulated AODs are realistic in the region of
31 interest, we compare the mean AOD from each model's control run with station observations



1 in Asia from the AERONET radiometer network (Holben et al., 2001). Because of the
2 limited number of stations in the region with long data records, we use the observed AOD at
3 500 nm from all AERONET stations able to provide an annual mean estimate for at least one
4 year, averaged over all years for which an annual mean was available, (generally ranging
5 between 1998 and 2014 in different stations), and compare this with the annual mean AODs
6 at 550 nm from the three models, masked to the locations of the AERONET stations
7 (Supplementary fig. S2). Focusing on stations in E. China (eight in total), we find that
8 HadGEM3-GA4 compares best with AERONET in this region with a mean station bias of -
9 22%, whilst both GISS-E2 and CESM1 appear to be biased lower in this part of the world,
10 with mean biases of -56% and -60% respectively.

11 We also calculate the area-weighted mean AOD as observed by the MODIS and MISR
12 satellite instruments. The MODIS (Moderate Resolution Imaging Spectroradiometer)
13 instrument is flown on both the Terra and Aqua satellites, whilst MISR (Multi-angle Imaging
14 SpectroRadiometer) is flown on Terra. For MODIS we use the collection 6 combined Deep
15 Blue + Dark Target monthly AOD product at 550 nm (Levy et al., 2013) (available from
16 <https://ladsweb.nascom.nasa.gov/>), averaged from both Terra and Aqua satellites, and take a
17 10-year average from 2003-2012 (2003 being the earliest year that data from both satellites is
18 available). For MISR we use the best estimate monthly AOD product (Kahn et al., 2010)
19 version 31 (available from <https://eosweb.larc.nasa.gov/>) at 550 nm over a 15-year averaging
20 period, from 2000-2014 (2000 being the earliest year MISR data is available). For MODIS
21 the area-weighted E. China mean AOD is 0.51, whilst for MISR it is 0.31, so regionally there
22 is a considerable uncertainty in these observations. HadGEM3-GA4 overestimates the AOD
23 compared with both instruments, with a regional average AOD of 0.58, whilst GISS-E2 and
24 CESM1 underestimate with regionally-averaged AODs of 0.23 for both models. Globally the
25 two instruments are in better agreement, with MODIS giving a global average AOD of 0.17
26 and MISR giving 0.15. Again HadGEM3-GA4 overestimates global AOD compared with
27 both instruments (0.22) whilst GISS-E2 and CESM1 both underestimate (0.13 and 0.12).
28 Given that CESM1 diagnosed all-sky AOD, whereas satellite retrievals are only possible for
29 clear-sky conditions, the underestimate for this model is likely greater than these numbers
30 suggest.

31 There is considerable variation in the observations as well as the models. Globally GISS-E2
32 seems to compare best against MODIS and MISR, though tentatively HadGEM3-GA4 seems



1 to have the more accurate AOD over China, comparing best regionally with both AERONET
2 and MODIS, though poorer against MISR. This suggests that the more concentrated sulfate
3 aerosol burden and larger AOD reduction simulated by HadGEM3-GA4 over this region may
4 be more realistic. However we note though that since these observations only measure total
5 AOD and cannot differentiate by species, the comparison cannot show for certain that the
6 higher sulfate optical depth specifically is more realistic in HadGEM3-GA4. The AOD
7 reduction over E. China due to removing Chinese SO₂ represents 50% of the climatological
8 total AOD in HadGEM3-GA4 over the region, compared with 34% in CESM1 and only 20%
9 in GISS-E2. Even if the total AOD in HadGEM3-GA4 is more realistic, there is still
10 considerable variation between the models as to what fraction of that total AOD is due to
11 Chinese SO₂ emissions.

12 For HadGEM3-GA4 and GISS-E2, for which sulfate mixing-ratio diagnostics were available
13 for individual model levels, we therefore also compared against the surface sulfate
14 observations conducted in China reported by Zhang et al. (2012) for 2006-2007
15 (Supplementary fig. S3). However, both models performed extremely poorly, with
16 HadGEM3-GA4 having a mean bias of -71% (-66% if urban stations are excluded), and
17 GISS-E2 having a mean bias of -87% (-86% when urban stations are excluded). Although
18 HadGEM3-GA4 is closer to the observed value, the large underestimation despite the
19 relatively good column AOD comparison suggests that the model has difficulty representing
20 the vertical profile of sulfate aerosol, and so this comparison with surface measurements may
21 not be that useful in constraining the sulfate optical depth or column-integrated burdens.
22 Large underestimations of surface sulfate concentration over East Asia have been reported
23 previously for two other models, MIROC and NICAM, by Goto et al. (2015), suggesting that
24 this is a problem common to many current generation models.

25 It seems plausible that any differences in the processing of sulfate aerosol would apply to all
26 polluted regions, and not just over China. Indeed, the spatial pattern of the climatological
27 sulfate burden over other major emission regions like the United States shows a similar
28 characteristic to that over China, with HadGEM3-GA4 having a higher burden close to the
29 emission source regions, whilst GISS-E2 has a more diffuse sulfate distribution
30 (Supplementary fig. S4). With this in mind we also validated these two models against
31 surface sulfate observations from the Interagency Monitoring of Protected Visual
32 Environments (IMPROVE) network in the United States (Malm et al., 1994), a dataset with a



1 far more extensive record than the Zhang et al. (2012) dataset for China. Taking 61
2 IMPROVE stations which have data for at least 6 years between 1995 and 2005, we find that
3 over the United States both models are biased slightly high, with GISS-E2 performing
4 relatively better with a mean bias of +10.1%, but HadGEM3-GA4 somewhat worse with
5 +44.5%. However, we find that the larger mean bias in HadGEM3-GA4 comes mainly from
6 an incorrect spatial distribution (Supplementary fig. S5), with a high bias on the West Coast
7 but a pronounced low bias in surface SO₄ on the East Coast. Consequently, this comparison
8 would suggest that HadGEM3-GA4 in fact has too little sulfate around the principal US
9 emission regions on the East Coast, even though over that area HadGEM3-GA4 actually has a
10 larger column-integrated sulfate burden (Supplementary fig. S4) and a larger AOD (not
11 shown) than GISS-E2, as was the case for China.

12 Validation with surface observations therefore seems insufficient to constrain which model
13 performs better with regard to the more climate-relevant column-integrated quantities of
14 sulfate burden and AOD. Returning to Asia, we therefore also tried validating HadGEM3-
15 GA4 and GISS-E2 using sulfate wet deposition observations, which should be less sensitive
16 to the precise vertical profile of sulfate in the models. We use the 3-year mean wet deposition
17 data from 2000-2002 described in Vet et al. (2014) and provided by the World Data Centre
18 for Precipitation Chemistry (<http://wdcpc.org>, 2014), taking the 6 stations located in China.
19 We exclude the station in Guizhou province in southern China where HadGEM3-GA4 has a
20 bias of +590% and GISS-E2 a bias of +253%. This station only provided data for one year
21 and was flagged as having a high uncertainty in the Vet et al. (2014) dataset; it is also located
22 in a mountainous region and so it could equally be that the models cannot resolve the specific
23 local conditions. Removing this station from the analysis we find for the remaining 5 stations
24 in China that HadGEM3-GA4 performs well with a mean bias of -3.9%, compared with -
25 64.8% for GISS-E2. This gives an indication that HadGEM3-GA4 has more realistic sulfate
26 deposition directly over China, though the sample size is very small. If we broaden the
27 analysis to include all stations described as being broadly in Asia – an additional 32 stations –
28 then the mean bias for HadGEM3-GA4 is worsened (-41.8%), whilst the bias in GISS-E2 is
29 slightly improved (-54.1%). HadGEM3-GA4 still performs better over the Asian region as a
30 whole, though less dramatically so (Supplementary fig. S6).

31

32 4.2 Differences in cloud effects



1 Sulfate aerosol exerts indirect radiative effects by modifying cloud properties. The strength
2 of these indirect effects is highly uncertain (e.g. Boucher et al., 2013) and differs substantially
3 between the models, having been shown to contribute substantially to inter-model variation in
4 historical aerosol forcing (Wilcox et al., 2015). Differences in the underlying climatologies of
5 the models, particularly with regard to cloud distributions, could also be important since the
6 radiative effect of sulfate aerosol is modulated by the reflectivity of the underlying surface in
7 the radiation scheme (Chýlek and Coakley, 1974; Chand et al., 2009), which may often be a
8 cloud-top.

9 In our case, the good correspondence between higher (clear-sky) AOD change in HadGEM3-
10 GA4 and higher (all-sky) SW flux change in this model would suggest that the cloud effects
11 are not the root cause of the larger radiative response in this model.

12 Additionally clear-sky SW flux diagnostics were available for HadGEM3-GA4 and GISS-E2
13 (Supplementary fig. S7), and comparing them with the all-sky SW flux anomalies we still find
14 a large - albeit smaller (3-fold rather than 6-fold) - discrepancy between these two models.
15 This reduced difference between GISS-E2 and HadGEM3-GA4 in the clear-sky compared
16 with all-sky anomaly is hard to apportion, because the all-sky response incorporates both
17 aerosol indirect effects and also dynamical feedbacks on clouds. In fact, in both models the
18 clear-sky SW change turns out to be larger than the all-sky SW change, which is opposite to
19 what we would expect from a simple amplification of the radiative response due to indirect
20 effects. In particular GISS-E2 simulates an increase in cloudiness in East China when sulfate
21 is removed (not shown), which partially offsets the direct forcing of reduced SO₄ and results
22 in a smaller all-sky flux change than clear-sky flux change (0.91 Wm⁻² compared with 1.8
23 Wm⁻²). HadGEM3-GA4 has mixed changes in cloud amount over East Asia (not shown) and
24 has a smaller difference between all-sky and clear-sky flux changes (5.3 Wm⁻² and 5.8 Wm⁻²
25 respectively), explaining why there is a bigger discrepancy between these two models in the
26 all-sky forcing. Nonetheless, the fact that there is still a 3-fold difference in clear-sky flux
27 indicates that even in a cloud-free world, there would be large disagreement in the models'
28 SW forcing over China, and so cloud responses are not the primary driver of the
29 discrepancies, although cloud feedbacks are clearly important in modulating the final
30 magnitude of the discrepancy.

31 Diagnostics for clear-sky radiative fluxes and cloud amount were not available for CESM1, so
32 we are unable to make a similar comparison for this model.



1

2 **4.3 Differences in aerosol forcing efficiency**

3 An additional source of discrepancy between the models lies in differences in the aerosol
4 radiative forcing efficiency – the forcing that results from a given aerosol optical depth or
5 burden (e.g. Samset et al, 2013). A previous model intercomparison looking at radiative
6 forcing as part of the AeroCom Phase II study found that there was a large variation in the
7 radiative forcing due to aerosol-radiation interactions per unit AOD between different
8 participating models (Myhre et al., 2013a) on a global scale.

9 Globally-averaged, the changes in radiative flux and AOD are too small in our experiments to
10 calculate an accurate ratio, but instead we calculate here a regional radiative efficiency for
11 HadGEM3-GA4 and GISS-E2 by taking the change in clear-sky SW flux over the 100-120E,
12 20-40N region (Sect. 4.2), and dividing by the clear-sky AOD change over the same region
13 (Table 1). This is not directly comparable with previous studies like Myhre et al. (2013a), as
14 we use a regionally-averaged number instead of globally-averaged, and for the numerator we
15 use the change in clear-sky SW flux rather than the clear-sky radiative forcing. Consequently
16 we use this metric here mainly to qualitatively highlight differences between the models.

17 As noted in Sect. 4.1 and 4.2, over the eastern China region HadGEM3-GA4 has a 6-fold
18 larger mean AOD reduction (-0.29) compared with GISS-E2 (-0.047), but only a 3-fold larger
19 clear-sky SW change (5.8 W m^{-2} compared with 1.8 W m^{-2}). As a result the regional radiative
20 efficiency for HadGEM3-GA4 is only about half that of GISS-E2 (-20.3 W m^{-2} compared
21 with -39.1 W m^{-2}). If we normalise by the change in sulfate burden instead of the AOD
22 integrated over the same region, however, we find the opposite relationship: HadGEM3-GA4
23 has a larger regional mean change in clear-sky SW flux per Tg sulfate than GISS-E2 (-167.1
24 $\text{W m}^{-2} \text{ Tg}^{-1}$ compared with $-117.7 \text{ W m}^{-2} \text{ Tg}^{-1}$). The much larger AOD per unit mass of
25 sulfate simulated in HadGEM3-GA4 therefore outweighs the smaller radiative response per
26 unit AOD. Curiously Myhre et al. (2013a) reported results that were qualitatively the inverse
27 of what we show here, finding that the atmospheric component of GISS ModelE2 has a
28 smaller sulfate radiative forcing than that of HadGEM2 (HadGEM3's predecessor, with a
29 very similar aerosol scheme) when normalised by AOD, but larger when normalised by
30 column-integrated sulfate burden. The reason for the discrepancy is not clear, though the
31 aforementioned fact that we calculate our numbers for a specific region means that there may



1 be important local factors. For instance, the forcing per unit AOD will be influenced by the
2 vertical distribution of the aerosol (Myhre et al., 2013a), which could vary between models in
3 different parts of the world.

4 Making an equivalent comparison for CESM1 is hindered by the lack of clear-sky diagnostics
5 available from this model for these simulations. What we can note is that if we instead use
6 the all-sky change in SW flux over East China, normalising by AOD we find a much larger
7 SW change per unit AOD in CESM1 than in HadGEM3-GA4 or GISS-E2 (-55.0 W m^{-2}
8 compared with -18.6 W m^{-2} and -19.6 W m^{-2}) (Table 1). Normalising by all-sky AOD in
9 GISS-E2 (which provides both clear-sky and all-sky diagnostics) however gives a
10 comparatively even smaller value (-4.95 W m^{-2}). Normalised by the change in regional
11 sulfate burden instead, CESM1 sits in the middle with $-107.7 \text{ W m}^{-2} \text{ Tg}^{-1}$, compared with
12 HadGEM3-GA4's $-153.5 \text{ W m}^{-2} \text{ Tg}^{-1}$ (quite close to its clear-sky normalised value), and
13 GISS-E2's $-56.6 \text{ W m}^{-2} \text{ Tg}^{-1}$ (much smaller than its clear-sky normalised value). These
14 results suggest that either CESM1 has a large radiative efficiency per unit AOD which
15 compensates for its much smaller AOD per mass of sulfate, or else there are large cloud
16 responses – either due to a particularly strong aerosol indirect effect, or a dynamical reduction
17 in local cloudiness – which considerably amplify the radiative effect of a relatively small
18 AOD reduction in this model.

19 The Myhre et al. (2013a) AeroCom intercomparison found that globally, the atmospheric
20 component of CESM1 (CAM5.1) did indeed have a much higher sulfate radiative efficiency
21 than the atmosphere-only version of GISS-E2. In their case, they found CAM5.1 to have
22 approximately 2.25 times higher direct radiative forcing per unit AOD than GISS-E2.
23 However, the study also found that, globally, the atmospheric component of HadGEM2 had a
24 very similar forcing efficiency to CAM5.1. Given that our regional values from GISS-E2 and
25 HadGEM3-GA4 conflict qualitatively with the global values from the AeroCom study
26 though, this probably does not provide a strong indication of which factor is more likely the
27 dominant driver of the relatively large response in CESM1 despite its modest AOD change.

28

29 **4.4 Differences in climate sensitivity**

30 So far we have discussed mainly factors which influence the translation of a change in aerosol
31 precursor emissions to a radiative heating, and these varied strongly between the models.



1 There is a final step in arriving at the climate response, which is the translation of a given
2 radiative heating into a surface temperature change. The climate sensitivity – the amount of
3 warming simulated per unit radiative forcing – is also well known to vary considerably
4 between models, globally (Flato et al., 2013) and regionally (Voulgarakis and Shindell, 2010),
5 and this will additionally impact the strength of the final response. Climate sensitivity is
6 typically estimated from a 2x or 4x global CO₂ simulation, giving a large response and a large
7 forcing from which to calculate the ratio. For GISS-E2, a climate sensitivity value of 0.6 K
8 (W m⁻²)⁻¹ was found in the IPCC AR5 report from a 4x CO₂ simulation (Flato et al., 2013)
9 using the regression method of Gregory et al. (2004) to estimate radiative forcing. For
10 CESM1, a value of 1.1 K (W m⁻²)⁻¹ is obtained from values from a 2x CO₂ simulation (Meehl
11 et al., 2013), noting that in this case the radiative forcing was calculated using the
12 stratospheric adjustment method (Hansen et al., 2005). For HadGEM3-GA4, we use a 100-
13 year 2x CO₂ simulation that was performed separately as part of the Precipitation Driver
14 Response Model Intercomparison Project (Samset et al., in preparation), which gives a value
15 of 1.1 K (W m⁻²)⁻¹ based on the Gregory method.

16 While CESM1 and HadGEM3-GA4 both have very similar climate sensitivities, we see that
17 GISS-E2 has a particularly small sensitivity – in fact, the smallest value of all the CMIP5
18 models reported in the AR5 report (Flato et al., 2013). This presumably compounds the fact
19 that GISS-E2 simulates the smallest SW flux change of the three models, ensuring that the
20 resulting surface temperature response is comparatively smaller still. Differences in climate
21 sensitivity do not seem to explain any of the variation in the magnitude of the response
22 between CESM1 and HadGEM3-GA4, at least based on these values. However, it is worth
23 noting that the climate sensitivity values that we report are derived from global CO₂ forcings,
24 whereas in our case we are looking at the translation of a very regional forcing into a global
25 response. It is not trivial that the global-mean temperature response to a regionally localised
26 forcing is a function only of the resulting globally-averaged forcing, and in particular it may
27 be that different models are more or less sensitive to forcings in specific regions.
28 Unfortunately we know of no study that has calculated climate sensitivity to regional forcings
29 in single or multi-model frameworks. Shindell (2012) calculated regional climate sensitivities
30 to forcings imposed in different latitudinal bands for the GISS-E2 model, finding that there is
31 considerable regional variation relative to the global climate sensitivity. In that study,
32 estimates of the response to regional forcings in 3 other global climate models, based on the
33 GISS-E2 regional sensitivities, are found to largely agree to within +/- 20% with the full



1 simulations however, suggesting that regional sensitivities (relative to a model's global
2 sensitivity) may not vary that much between models.

3

4 **5 Conclusions**

5 By applying an identical regional perturbation to anthropogenic SO₂ emissions in three
6 different climate models, we observe three markedly different resulting climate responses,
7 ranging from virtually no coherent surface air temperature response in one model (GISS-E2),
8 to pronounced surface warming all across most of the northern hemisphere in another
9 (HadGEM3-GA4). The third model (CESM1) sits in the middle in terms of both magnitude
10 and spatial extent of the temperature response. This huge variation in climate response
11 corresponds to a similarly large variation in the SW radiative flux change following the
12 reduction in sulfate aerosol. All three models show a fairly localised increase in net
13 downwards SW radiation over China as a result of reduced SO₂ emissions from this region,
14 however the magnitude of this radiative heating is substantially greater in HadGEM3-GA4
15 than in CESM1, which is substantially greater still than in GISS-E2. The response in GISS-
16 E2 is so weak that temperature changes are largely not detectable above the internal
17 variability of the model. The stronger heating in CESM1 and HadGEM3-GA4 produces
18 much more pronounced temperature changes, and even though the radiative heating is
19 localised over China, the temperature responses in these two models are much more spread
20 out, particularly in the zonal direction. This is consistent with the findings of Shindell et al.
21 (2010), who found that the temperature response to inhomogeneous aerosol forcings is more
22 uniform and extends much further from the forcing location in the zonal direction than in the
23 meridional direction.

24 Comparing the models we find very different changes in the SO₄ mass change due to
25 removing SO₂ emissions from China, very different ratios of AOD change per mass of sulfate,
26 and different radiative flux changes per unit AOD. These differences are compounded further
27 by variations in cloud responses, climate sensitivity, and the feedbacks on other aerosol
28 species such as nitrate, which diversify the response further. In addition to differences in the
29 total changes in sulfate and AOD, we find there are also substantial differences in the spatial
30 distribution of the changes, attributed to differences in the rate of chemical conversion of SO₂
31 to SO₄ which influences how concentrated the aerosol changes are around the emission



1 region. This implies that even if both the AOD per sulfate burden and the forcing per unit
2 AOD were identical among the three models, they would still have different distributions of
3 radiative forcing.

4 Specifically, we find that CESM1 simulates the largest reduction in sulfate burden both
5 globally and locally. HadGEM3-GA4 has the smallest reduction in sulfate burden globally
6 and the second largest reduction regionally, yet it produces by far the largest reduction in
7 AOD both globally and regionally over E. China. This much larger change in AOD per
8 change in sulfate burden in HadGEM3-GA4 results in the largest radiative changes and the
9 largest temperature response in this model. Though both GISS-E2 and CESM1 simulate
10 much smaller changes in AOD than HadGEM3-GA4, still the SW flux changes and
11 temperature responses produced are very different between these two models. In GISS-E2 the
12 radiative effect of sulfate burden changes appears smallest, and this combines with
13 compensating increases in local cloud amount over China and nitrate aerosol globally to
14 reduce the radiative response yet further, and a smaller climate sensitivity results in this being
15 translated into a largely negligible temperature response.

16 There are no direct observations of sulfate radiative forcing, nor of sulfate optical depth or
17 vertically-integrated burden, and so we have tried validating the aerosol component of the
18 models with a range of surface and satellite-based measurements of total aerosol optical
19 depth, surface sulfate concentration, and sulfate wet deposition. All the models have biases,
20 and no model performs best against all the observational datasets used. Tentatively
21 HadGEM3-GA4 seems to perform best over China against observations of both total AOD
22 and sulfate wet deposition, though over some other parts of the world this model performed
23 slightly poorer, e.g. for global AOD and US surface sulfate concentrations. However, the
24 main conclusion is that comparison against all existing observational measures is unable to
25 satisfactorily constrain which model response is more realistic. The model with the largest
26 sulfate mass change (CESM1) did not have the largest radiative or climate response, and two
27 models with a similar AOD change (CESM1 and GISS-E2) had markedly different radiative
28 and climate responses. Given the range of discrepancies that we find in all steps along the
29 conversion of SO₂ change to SO₄ change to AOD change to radiative forcing to temperature
30 response, it seems that knowing how accurate a model is with respect to either sulfate
31 concentrations or total AOD is far from sufficient to determine whether the climate response
32 to a regional aerosol perturbation is similarly accurate.



1 We have only looked here at surface temperature, which is a particularly direct measure of the
2 climate response. The response of other, less well-constrained, climate variables such as
3 precipitation might be expected to show even greater variation. Our results show that there
4 remains a very large uncertainty in current climate models in the translation of aerosol
5 precursor emissions into a climate response, and imply that care must be taken not to over-
6 interpret the results of studies performed with single models.

7 On a more optimistic note, we remark that in the two models which showed the more
8 substantial change in SW radiative flux (CESM1 and HadGEM3-GA4), both also show a
9 remarkably strong remote temperature response to a relatively localised northern-midlatitude
10 heat source, with qualitatively similar temperature change patterns that extend across much of
11 the hemisphere, indicating that there may be some agreement on the response to a given
12 regional forcing, if not on the forcing itself.

13

14 **Data availability**

15 Model output data from all simulations described here is available upon request from the
16 corresponding author.

17

18 **Acknowledgements**

19 MK and AV are supported by the Natural Environment Research Council under grant number
20 NE/K500872/1. Also, we wish to thank the European Commission's Marie Curie Actions
21 International Research Staff Exchange Scheme (IRSES) for funding MK's placement at
22 NASA GISS and Columbia University and facilitating interactions on this work with the US
23 colleagues, as part of the Regional Climate-Air Quality Interactions (REQUA) project.
24 Simulations with GISS-E2 used resources provided by the NASA High-End Computing
25 (HEC) Program through the NASA Center for Climate Simulation (NCCS) at Goddard Space
26 Flight Center. Simulations with HadGEM3-GA4 were performed using the MONSooN
27 system, a collaborative facility supplied under the Joint Weather and Climate Research
28 Programme, which is a strategic partnership between the Met Office and the Natural
29 Environment Research Council. We specifically thank Dr. Fiona O'Connor, Dr. Jeremy



- 1 Walton, and Mr. Mohit Dalvi from the Met Office for their support with using the HadGEM3-
- 2 GA4 model.



1 **References**

- 2 Andreae, M. O. and Crutzen, P. J.: Atmospheric Aerosols: Biogeochemical Sources and Role
3 in Atmospheric Chemistry, *Science*, 276, 1052-1058, 1997.
- 4 Andres, R. J. and Kasgnoc, A. D.: A time-averaged inventory of subaerial volcanic sulfur
5 emissions, *J. Geophys. Res.*, 103, D19, 25251-25261, 1998.
- 6 Andrews, T., Forster, P. M., Boucher, O., Bellouin, N., and Jones, A.: Precipitation, radiative
7 forcing and global temperature change, *Geophys. Res. Lett.*, 37, L14701,
8 doi:10.1029/2010GL043991, 2010.
- 9 Bellouin, N., Boucher, O., Haywood, J., Johnson, C., Jones, A., Rae, J., and Woodward, S.:
10 Improved representation of aerosols for HadGEM2, Technical Note 73, Hadley Centre, Met
11 Office, Exeter, UK, 2007.
- 12 Bellouin, N., Rae, J., Jones, A., Johnson, C., Haywood, J., and Boucher, O.: Aerosol forcing
13 in the Climate Model Intercomparison Project (CMIP5) simulations by HadGEM2-ES and the
14 role of ammonium nitrate, *J. Geophys. Res.*, 116, D20206, doi:10.1029/2011JD016074, 2011.
- 15 Bollasina, A. M., Ming, Y., and Ramaswamy, V.: Anthropogenic Aerosols and the
16 Weakening of the South Asian Summer Monsoon, *Science*, 334, 502-505, 2011.
- 17 Booth, B., Dunstone, N. J., Halloran, P. R., Andrews, T., and Bellouin, N.: Aerosols
18 implicated as a prime driver of twentieth-century North Atlantic climate variability, *Nature*,
19 484, 228-232, doi:10.1038/nature10946, 2012.
- 20 Boucher, O., Randall, D., Artaxo, P., Bretherton, C., Feingold, G., Forster, P., Kerminen, V.-
21 M., Kondo, Y., Liao, H., Lohmann, U., Rasch, P., Satheesh, S. K., Sherwood, S., Stevens, B.,
22 and Zhang, X. Y.: Clouds and Aerosols. In: *Climate Change 2013: The Physical Science
23 Basis. Contribution of Working Group I to the Fifth Assessment Report of the
24 Intergovernmental Panel on Climate Change* [Stocker, T. F., Qin, D., Plattner, G.-K., Tignor,
25 M., Allen, S. K., Boschung, J., Nauels, A., Xia, Y., Bex, V., and Midgley, P. M. (eds.)],
26 Cambridge University Press, Cambridge, United Kingdom and New York, NY, USA, 2013.
- 27 Chand, D., Wood, R., Anderson, T. L., Satheesh, S. K., and Charlson, R. J.: Satellite derived
28 direct radiative effect of aerosols dependent on cloud cover, *Nature Geosci.*, 2, 181-184,
29 2009.



- 1 Chýlék, P. and Coakley, J. A. Jr.: Aerosol and climate, *Science*, 183, 75-77, 1974.
- 2 Cionni, I., Eyring, V., Lamarque, J. F., Randel, W. J., Stevenson, D. S., Wu, F., Bodeker, G.
3 E., Shepherd, T. G., Shindell, D. T., and Waugh, D. W.: Ozone database in support of CMIP5
4 simulations: results and corresponding radiative forcing, *Atmos. Chem. Phys.*, 11, 11267-
5 11292, doi:10.5194/acp-11-11267-2011, 2011.
- 6 Derwent, R. G., Collins, W. J., Jenkin, M. E., Johnson, C. E., and Stevenson, D. S.: The
7 global distribution of secondary particulate matter in a 3D Lagrangian chemistry transport
8 model, *J. Atmos. Chem.*, 44, 57-95, 2003.
- 9 Dong, B., Sutton, R. T., Highwood, E., and Wilcox, L.: The Impacts of European and Asian
10 Anthropogenic Sulfur Dioxide Emissions on Sahel Rainfall, *J. Climate*, 27, 7000-7017,
11 doi:10.1175/JCLI-D-13-00769.1, 2014.
- 12 Flato, G., Marotzke, J., Abiodun, B., Braconnot, P., Chou, S. C., Collins, W., Cox, P.,
13 Driouech, F., Emori, S., Eyring, V., Forest, C., Gleckler, P., Guilyardi, E., Jakob, C., Kattsov,
14 V., Reason, C., and Rummukainen, M.: Evaluation of Climate Models. In: *Climate Change*
15 *2013: The Physical Science Basis. Contribution of Working Group I to the Fifth Assessment*
16 *Report of the Intergovernmental Panel on Climate Change* [Stocker, T. F., Qin, D., Plattner,
17 G.-K., Tignor, M., Allen, S. K., Boschung, J., Nauels, A., Xia, Y., Bex, V., and Midgley, P.
18 M. (eds.)], Cambridge University Press, Cambridge, United Kingdom and New York, NY,
19 USA, 2013.
- 20 Gregory, J. M., Ingram, W. J., Palmer, M. A., Jones, G. S., Stott, P. A., Thorpe, R. B., Lowe,
21 J. A., Johns, T. C., and Williams, K. D.: A new method for diagnosing radiative forcing and
22 climate sensitivity, *Geophys. Res. Lett.*, 31, L03205, doi:10.1029/2003GL018747, 2004.
- 23 Hansen, J., Sato, M., Ruedy, R., Nazarenko, L., Lacis, A., Schmidt, G. A., Russell, G.,
24 Aleinov, I., Bauer, M., Bauer, S., Bell, N., Cairns, B., Canuto, V., Chandler, M., Cheng, Y.,
25 Del Genio, A., Faluvegi, G., Fleming, E., Friend, A., Hall, T., Jackman, C., Kelley, M.,
26 Kiang, N., Koch, D., Lean, J., Lerner, J., Lo, K., Menon, S., Miller, R., Minnis, P., Novakov,
27 T., Oinas, V., Perlwitz, Ja., Perlwitz, Ju., Rind, D., Romanou, A., Shindell, D., Stone, P., Sun,
28 S., Tausnev, N., Thresher, D., Wielicki, B., Wong, T., Yao, M., and Zhang, S.: Efficacy of
29 climate forcings, *J. Geophys. Res.*, 110, D18104, doi:10.1029/2005JD005776, 2005.



- 1 Hemispheric Transport of Air Pollution (HTAP): Hemispheric Transport of Air Pollution
2 2010. Part A: Ozone and Particulate Matter, Air Pollution Studies No. 17, [Dentener, F.,
3 Keating, T., and Akimoto, H. (eds.)], United Nations, New York, 2010.
- 4 Holben, B. N., Tanré, D., Smirnov, A., Eck, T. F., Slutsker, I., Abuhassan, N., Newcomb, W.
5 W., Schafer, J. S., Chatenet, B., Lavenu, F., Kaufman, Y. J., Vande Castle, J., Setzer, A.,
6 Markham, B., Clark, D., Frouin, R., Halthore, R., Karneli, A., O'Neill, N. T., Pietras, C.,
7 Pinker, R. T., Voss, K., and Zibordi, G.: An emerging ground-based aerosol climatology:
8 Aerosol optical depth from AERONET, *J. Geophys. Res.*, 106(D11), 12067–12097,
9 doi:10.1029/2001JD900014, 2001.
- 10 Hunke, E. C. and Lipscombe, W. H.: CICE: the Los Alamos sea ice model documentation and
11 software user's manual, Version 4.0, LA-CC-06-012, Los Alamos National Laboratory, New
12 Mexico, 2008.
- 13 Hwang, Y.-T., Frierson, D. M. W., and Kang, S. M.: Anthropogenic sulfate aerosol and the
14 southward shift of tropical precipitation in the late 20th century, *Geophys. Res. Lett.*, 40,
15 doi:10.1002/grl.50502, 2013.
- 16 Jones, A., Roberts, D. L., Woodage, M. J., and Johnson, C. E.: Indirect sulphate aerosol
17 forcing in a climate model with an interactive sulphur cycle, *J. Geophys. Res.*, 106, 20293–
18 20310, 2001.
- 19 Kinne, S., Schulz, M., Textor, C., Guibert, S., Balkanski, Y., Bauer, S. E., Berntsen, T.,
20 Berglen, T. F., Boucher, O., Chin, M., Collins, W., Dentener, F., Diehl, T., Easter, R.,
21 Feichter, J., Fillmore, D., Ghan, S., Ginoux, P., Gong, S., Grini, A., Hendricks, J.,
22 Herzog, M., Horowitz, L., Isaksen, I., Iversen, T., Kirkevåg, A., Kloster, S., Koch, D.,
23 Kristjansson, J. E., Krol, M., Lauer, A., Lamarque, J. F., Lesins, G., Liu, X., Lohmann, U.,
24 Montanaro, V., Myhre, G., Penner, J., Pitari, G., Reddy, S., Seland, O., Stier, P.,
25 Takemura, T., and Tie, X.: An AeroCom initial assessment – optical properties in aerosol
26 component modules of global models, *Atmos. Chem. Phys.*, 6, 1815-1834, doi:10.5194/acp-6-
27 1815-2006, 2006.
- 28 Goto, D., Nakajima, T., Dai, T., Takemura, T., Kajino, M., Matsui, H., Takami, A.,
29 Hatakeyama, S., Sugimoto, N., Shimizu, A., and Ohara, T.: An evaluation of simulated
30 particulate sulfate over East Asia through global model intercomparison, *J. Geophys. Res.*
31 *Atmos.*, 120, doi:10.1002/2014JD021693, 2015.



- 1 Kahn, R. A., Gaitley, B. J., Garay, M. J., Diner, D. J., Eck, T. F., Smirnov, A., and Holben, B.
2 N.: Multiangle Imaging SpectroRadiometer global aerosol product assessment by comparison
3 with the Aerosol Robotic Network, *J. Geophys. Res.*, 115, D23209,
4 doi:10.1029/2010JD014601, 2010.
- 5 Koch, D., Schmidt, G. A., and Field, C. V.: Sulfur, sea salt and radionuclide aerosols in GISS
6 ModelE, *J. Geophys. Res.*, 111, doi:10.1029/2004JD005550, 2006.
- 7 Koch, D., Bauer, S., Del Genio, A., Faluvegi, G., McConnell, J. R., Menon, S., Miller, R. L.,
8 Rind, D., Ruedy, R., Schmidt, G. A., and Shindell, D.: Coupled aerosol-chemistry-climate
9 twentieth century transient model investigation: Trends in short-lived species and climate
10 responses, *J. Climate*, 24, 2693–2714, doi:10.1175/2011JCLI3582.1, 2011.
- 11 Lamarque, J.-F., Bond, T. C., Eyring, V., Granier, C., Heil, A., Klimont, Z., Lee, D.,
12 Liousse, C., Mieville, A., Owen, B., Schultz, M. G., Shindell, D., Smith, S. J., Stehfest, E.,
13 Van Aardenne, J., Cooper, O. R., Kainuma, M., Mahowald, N., McConnell, J. R., Naik, V.,
14 Riahi, K., and van Vuuren, D. P.: Historical (1850–2000) gridded anthropogenic and biomass
15 burning emissions of reactive gases and aerosols: methodology and application, *Atmos.*
16 *Chem. Phys.*, 10, 7017–7039, doi:10.5194/acp-10-7017-2010, 2010.
- 17 Lawrence, D.M., Oleson, K. W., Flanner, M. G., Thornton, P. E., Swenson, S. C., Lawrence,
18 P. J., Zeng, X., Yang, Z.-L., Levis, S., Sakaguchi, K., Bonan, G. B., and Slater, A.
19 G.: Parameterization improvements and functional and structural advances in version 4 of the
20 Community Land Model, *J. Adv. Model. Earth Sys.*, 3, DOI: 10.1029/2011MS000045, 2011.
- 21 Levy, R. C., Mattoo, S., Munchak, L. A., Remer, L. A., Sayer, A. M., Patadia, F., and Hsu, N.
22 C.: The Collection 6 MODIS aerosol products over land and ocean, *Atmos. Meas. Tech.*, 6,
23 2989–3034, doi:10.5194/amt-6-2989-2013, 2013.
- 24 Liu, X., Easter, R. C., Ghan, S., Zaveri, R., Rasch, P., Shi, X., Lamarque, J.-F., Gettelman, A.,
25 Morrison, H., Vitt, F., Conley, A., Park, S., Neale, R., Hannay, C., Ekman, A. M. L., Hess, P.,
26 Mahowald, N, Collins, W., Iacono, M. J., Bretherton, C. S., Flanner, M. G., and Mitchell, D.,
27 Toward a Minimal Representation of Aerosol Direct and Indirect Effects: Model Description
28 and Evaluation, *GeoSci. Mod. Dev.*, 5, 709–739, doi:10.5194/gmd-5-709-2012, 2012.
- 29 Madec, G.: NEMO ocean engine, Institut Piere-Simon Laplace (IPSL), France, No. 27, ISSN
30 No. 1288–1619, 2008.



- 1 Malm, W. C., Sisler, J. F., Huffman, D., Eldred, R. A., and Cahill, T. A.: Spatial and seasonal
2 trends in particle concentration and optical extinction in the United States, *J. Geophys. Res.*,
3 99, 1347–1370, 1994.
- 4 Meehl, G. A., Washington, W. M., Arblaster, J. M., Hu, A., Teng, H., Kay, J. E., Gettleman,
5 A., Lawrence, D. M., Sanderson, B. M., and Strand, W. G.: Climate Change Projections in
6 CESM1(CAM5) Compared to CCMS4, *Journal of Climate*, 26, 6287-6308, 2013.
- 7 Menon, S., Koch, D., Beig, G., Sahu, S., Fasullo, J., and Orlikowski, D.: Black carbon
8 aerosols and the third polar ice cap, *Atmos. Chem. Phys.*, 10, 4559–4571, 2010.
- 9 Miller, R. L., Schmidt, G. A., Nazarenko, L. S., Tausnev, N., Bauer, S. E., Del Genio, A. D.,
10 Kelley, M., Lo, K. K., Ruedy, R., Shindell, D. T., Aleinov, I., Bauer, M., Bleck, R., Canuto,
11 V., Chen, Y.-H., Cheng, Y., Clune, T. L., Faluvegi, G., Hansen, J. E., Healy, R. J., Kiang, N.
12 Y., Koch, D., Lacis, A. A., LeGrande, A. N., Lerner, J., Menon, S., Oinas, V., Pérez García-
13 Pando, C., Perlwitz, J. P., Puma, M. J., Rind, D., Romanou, A., Russell, G. L., Sato, M., Sun,
14 S., Tsigaridis, K., Unger, N., Voulgarakis, A., Yao, M.-S., and Zhang, J.: CMIP5 historical
15 simulations (1850-2012) with GISS ModelE2, *J. Adv. Model. Earth Syst.*, 6, no. 2, 441-477,
16 doi:10.1002/2013MS000266, 2014.
- 17 Myhre, G., Samset, B. H., Schulz, M., Balkanski, Y., Bauer, S., Berntsen, T. K., Bian, H.,
18 Bellouin, N., Chin, M., Diehl, T., Easter, R. C., Feichter, J., Ghan, S. J., Hauglustaine, D.,
19 Iversen, T., Kinne, S., Kirkevåg, A., Lamarque, J.-F., Lin, G., Liu, X., Lund, M. T., Luo, G.,
20 Ma, X., van Noije, T., Penner, J. E., Rasch, P. J., Ruiz, A., Seland, Ø., Skeie, R. B., Stier, P.,
21 Takemura, T., Tsigaridis, K., Wang, P., Wang, Z., Xu, L., Yu, H., Yu, F., Yoon, J.-H.,
22 Zhang, K., Zhang, H., and Zhou, C.: Radiative forcing of the direct aerosol effect from
23 AeroCom Phase II simulations, *Atmos. Chem. Phys.*, 13, 1853-1877, doi:10.5194/acp-13-
24 1853-2013, 2013a.
- 25 Myhre, G., Shindell, D., Breon, F.-M., Collins, W., Fuglestedt, J., Huang, J., Koch, D.,
26 Lamarque, J.-F., Lee, D., Mendoza, B., Nakajima, T., Robock, A., Stephens, G., Takemura,
27 T., and Zhang, H.: Anthropogenic and Natural Radiative Forcing. In: *Climate Change 2013:
28 The Physical Science Basis. Contribution of Working Group I to the Fifth Assessment Report
29 of the Intergovernmental Panel on Climate Change* [Stocker, T. F., Qin, D., Plattner, G.-K.,
30 Tignor, M., Allen, S. K., Boschung, J., Nauels, A., Xia, Y., Bex, V., and Midgley, P. M.



- 1 (eds.)], Cambridge University Press, Cambridge, United Kingdom and New York, NY, USA,
2 2013b.
- 3 Neale, R. B., Chen, C.-C., Gettleman, A., Lauritzen, P. H., Park, S., Williamson, D. L.,
4 Conley, A. J., Garcia, R., Kinnison, D., Lamarque, J.-F., Marsh, D., Mills, M., Smith, A. K.,
5 Tilmes, S., Vitt, F., Morrison, H., Cameron-Smith, P., Collins, W. D., Iacono, M. J., Easter,
6 R. C., Ghan, S. J., Liu, X., Rasch, P. J., and Taylor, M. A.: Description of the NCAR
7 Community Atmosphere Model (CAM 5.0), NCAR Technical Note TN-486+STR, National
8 Center for Atmospheric Research, Boulder, Colorado, USA, 2012.
- 9 Polson, D., Bollasina, M., Hegerl, G. C., and Wilcox, L. J.: Decreased monsoon precipitation
10 in the Northern Hemisphere due to anthropogenic aerosols, *Geophys. Res. Lett.*, 41,
11 doi:10.1002/2014GL060811, 2014.
- 12 Reddy, S., Seland, O., Stier, P., Takemura, T., and Tie, X.: An AeroCom initial assessment –
13 optical properties in aerosol component modules of global models, *Atmos. Chem. Phys.*, 6,
14 1815-1834, doi:10.5194/acp-6-1815-2006, 2006.
- 15 Russell, G. L., Miller, J. R., and Rind, D.: A coupled atmosphere-ocean model for transient
16 climate change, *Atmosphere-Ocean*, 33(4), 683–730, 1995.
- 17 Samset, B. H., Myhre, G., Schulz, M., Balkanski, Y., Bauer, S., Bernsten, T. K., Bian, H.,
18 Bellouin, N., Diehl, T., Easter, R. C., Ghan, S. J., Iversen, T., Kinne, S., Kirkevåg, A.,
19 Lamarque, J.-F., Lin, G., Liu, X., Penner, J. E., Seland, Ø., Skeie, R. B., Stier, P., Takemura,
20 T., Tsigaridis, K., and Zhang, K.: Black carbon vertical profiles strongly affect its radiative
21 forcing uncertainty, *Atmos. Chem. Phys.*, 13, 2423-2434, doi:10.5194/acp-13-2423-2013,
22 2013.
- 23 Samset et al., in preparation.
- 24 Schmidt, G.A., Kelley, M., Nazarenko, L., Ruedy, R., Russell, G. L., Aleinov, I., Bauer, M.,
25 Bauer, S. E., Bhat, M. K., Bleck, R., Canuto, V., Chen, Y.-H., Cheng, Y., Clune, T. L., Del
26 Genio, A., de Fainchtein, R., Faluvegi, G., Hansen, J. E., Healy, R. J., Kiang, N. Y., Koch, D.,
27 Lacis, A. A., LeGrande, A. N., Lerner, J., Lo, K. K., Matthews, E. E., Menon, S., Miller, R.
28 L., Oinas, V., Oloso, A. O., Perlwitz, J. P., Puma, M. J., Putman, W. M., Rind, D., Romanou,
29 A., Sato, M., Shindell, D. T., Sun, S., Syed, R. A., Tausnev, N., Tsigaridis, K., Unger, N.,
30 Voulgarakis, A., Yao, M.-S., and Zhang, J.: Configuration and assessment of the GISS



- 1 ModelE2 contributions to the CMIP5 archive, *J. Adv. Model. Earth Syst.*, 6, no. 1, 141-184,
2 doi:10.1002/2013MS000265, 2014.
- 3 Schulz, M., Textor, C., Kinne, S., Balkanski, Y., Bauer, S., Berntsen, T., Berglen, T.,
4 Boucher, O., Dentener, F., Guibert, S., Isaksen, I. S. A., Iversen, T., Koch, D., Kirkevåg, A.,
5 Liu, X., Montanaro, V., Myhre, G., Penner, J. E., Pitari, G., Reddy, S., Seland, Ø., Stier, P.,
6 and Takemura, T.: Radiative forcing by aerosols as derived from the AeroCom present-day
7 and pre-industrial simulations, *Atmos. Chem. Phys.*, 6, 5225-5246, doi:10.5194/acp-6-5225-
8 2006, 2006.
- 9 Shindell, D. T.: Evaluation of the absolute regional temperature potential, *Atmospheric*
10 *Chemistry and Physics*, 12, 7955-7960, doi:10.5194/acp-12-7955-2012, 2012.
- 11 Shindell, D. and Faluvegi, G.: Climate response to regional radiative forcing during the 20th
12 century, *Nat. Geosci.*, 2, 294-300, 2009.
- 13 Shindell, D., Schulz, M., Ming, Y., Takemura, T., Faluvegi, G., and Ramaswamy, V.: Spatial
14 scales of climate response to inhomogeneous radiative forcing, *J. Geophys. Res.*, 115,
15 D19110, doi:10.1029/2010JD014108, 2010.
- 16 Shindell, D. T., Voulgarakis, A., Faluvegi, G., and Milly, G.: Precipitation response to
17 regional radiative forcing, *Atmos. Chem. Phys.*, 12, 6969–6982, 2012.
- 18 Shindell, D. T., Lamarque, J.-F., Schulz, M., Flanner, M., Jiao, C., Chin, M., Young, P. J.,
19 Lee, Y. H., Rotstayn, L., Mahowald, N., Milly, G., Faluvegi, G., Balkanski, Y., Collins, W. J.,
20 Conley, A. J., Dalsoren, S., Easter, R., Ghan, S., Horowitz, L., Liu, X., Myhre, G.,
21 Nagashima, T., Naik, V., Rumbold, S. T., Skeie, R., Sudo, K., Szopa, S., Takemura, T.,
22 Voulgarakis, A., Yoon, J.-H., and Lo, F.: Radiative forcing in the ACCMIP historical and
23 future climate simulations, *Atmos. Chem. Phys.*, 13, 2939-2974, doi:10.5194/acp-13-2939-
24 2013, 2013a.
- 25 Shindell, D. T., Pechony, O., Voulgarakis, A., Faluvegi, G., Nazarenko, L., Lamarque, J.-F.,
26 Bowman, K., Milly, G., Kovari, B., Ruedy, R., and Schmidt, G.: Interactive ozone and
27 methane chemistry in GISS-E2 historical and future climate simulations, *Atmos. Chem.*
28 *Phys.*, 13, 2653-2689, doi:10.5194/acp-13-2653-2013, 2013b.



- 1 Shindell, D. T., Faluvegi, G., Rotstayn, L., and Milly, G.: Spatial patterns of radiative forcing
2 and surface temperature response, *J. Geophys. Res. Atmos.*, 120, doi:10.1002/2014JD022752,
3 2015
- 4 Smith, S. J., van Aardenne, J., Klimont, Z., Andres, R. J., Volke, A., and Delgado Arias, S.:
5 Anthropogenic sulfur dioxide emissions: 1850–2005, *Atmos. Chem. Phys.*, 11, 1101–1116,
6 doi:10.5194/acp-11-1101-2011, 2011.
- 7 Taylor, K. E., Stouffer, R. J., and Meehl, G. A.: An Overview of CMIP5 and the Experiment
8 Design, *Bull. Amer. Meteor. Soc.*, 93, 485–498, doi:10.1175/BAMS-D-11-00094.1, 2012.
- 9 Teng, H., Washington, W. M., Branstator, G., Meehl, G. A., and Lamarque, J.-F.: Potential
10 impacts of Asian carbon aerosols on future US warming, *Geophys. Res. Lett.*, 39, L11703,
11 doi:10.1029/2012GL051723, 2012.
- 12 Textor, C., Schulz, M., Guibert, S., Kinne, S., Balkanski, Y., Bauer, S., Bernsten, T.,
13 Berglen, T., Boucher, O., Chin, M., Dentener, F., Diehl, T., Easter, R., Feichter, H.,
14 Fillmore, D., Ghan, S., Ginoux, P., Gong, S., Grini, A., Hendricks, J., Horowitz, L.,
15 Huang, P., Isaksen, I., Iversen, I., Kloster, S., Koch, D., Kirkevåg, A., Kristjansson, J. E.,
16 Krol, M., Lauer, A., Lamarque, J. F., Liu, X., Montanaro, V., Myhre, G., Penner, J., Pitari, G.,
17 Reddy, S., Seland, Ø., Stier, P., Takemura, T., and Tie, X.: Analysis and quantification of the
18 diversities of aerosol life cycles within AeroCom, *Atmos. Chem. Phys.*, 6, 1777–1813,
19 doi:10.5194/acp-6-1777-2006, 2006.
- 20 Tilmes, S., Lamarque, J.-F., Emmons, L. K., Kinnison, D. E., Ma, P.-L., Liu, X., Ghan, S.,
21 Bardeen, C., Arnold, S., Deeter, M., Vitt, F., Ryerson, T., Elkins, J. W., Moore, F., and
22 Spackman, R.: Description and evaluation of tropospheric chemistry and aerosols in the
23 Community Earth System Model (CESM1.2), *Geosci. Model Dev.*, 8, 1395–1426,
24 doi:10.5194/gmd-8-1395-2015, 2015.
- 25 Vet, R., Artz, R. S., Carou, S., Shaw, M., Ro, C.-U., Aas, W., Baker, A., Bowersox, V. C.,
26 Dentener, F., Galy-Lacaux, C., Hou, A., Pienaar, J. J., Gillett, R., Forti, M. C., Gromov, S.,
27 Hara, H., Khodzher, T., Mahowald, N. M., Nickovic, S., Rao, P. S. P., and Reid, N. W.: A
28 global assessment of precipitation chemistry and deposition of sulfur, nitrogen, sea salt, base
29 cations, organic acids, acidity and pH, and phosphorus, *Atmospheric Environment*, 93, 3–100,
30 doi:10.1016/j.atmosenv.2013.10.060, 2014.



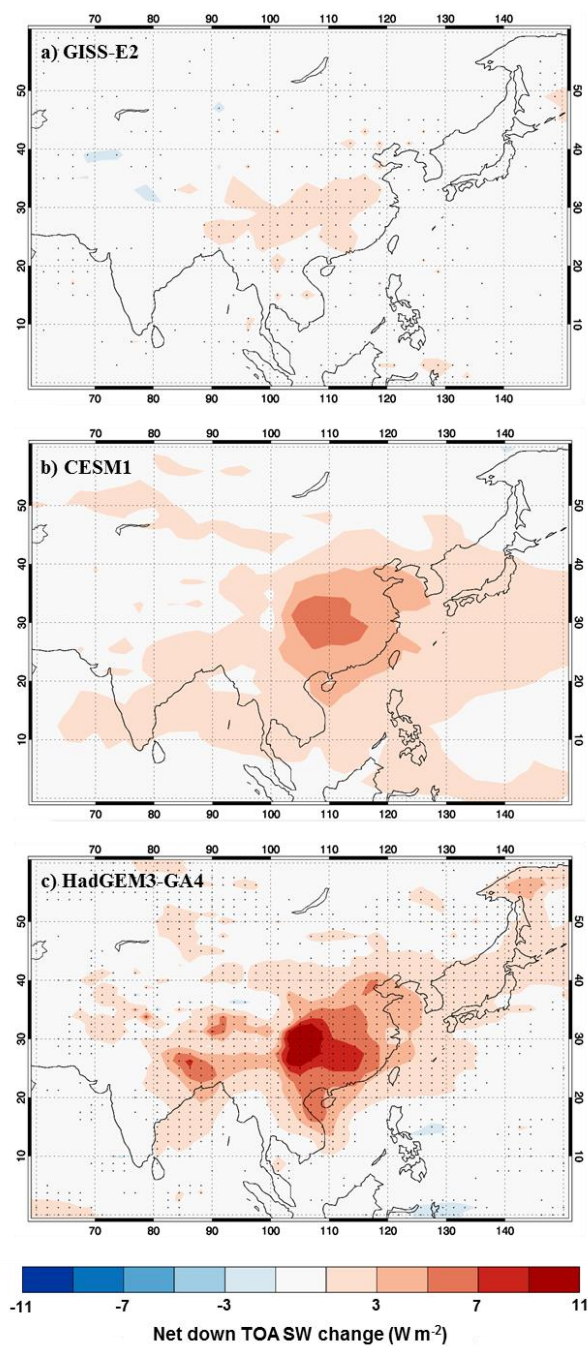
- 1 Voulgarakis, A., and Shindell, D. T., Constraining the sensitivity of regional climate with the
2 use of historical observations. *J. Climate*, 23, 6068-6073, doi:10.1175/2010JCLI3623.1, 2010.
- 3 Walters, D. N., Williams, K. D., Boutle, I. A., Bushell, A. C., Edwards, J. M., Field, P. R.,
4 Lock, A. P., Morcrette, C. J., Stratton, R. A., Wilkinson, J. M., Willett, M. R., Bellouin, N.,
5 Bodas-Salcedo, A., Brooks, M. E., Copsey, D., Earnshaw, P. D., Hardiman, S. C.,
6 Harris, C. M., Levine, R. C., MacLachlan, C., Manners, J. C., Martin, G. M., Milton, S. F.,
7 Palmer, M. D., Roberts, M. J., Rodríguez, J. M., Tennant, W. J., and Vidale, P. L.: The Met
8 Office Unified Model Global Atmosphere 4.0 and JULES Global Land 4.0 configurations,
9 *Geosci. Model Dev.*, 7, 361-386, doi:10.5194/gmd-7-361-2014, 2014.
- 10 Wilcox, L. J., Highwood, E. J., and Dunstone, N. J.: The influence of anthropogenic aerosol
11 on multi-decadal variations of historical global climate *Environ. Res. Lett.*, 8, 024033, 2013.
- 12 Wilcox, L. J., Highwood, E. J., Booth, B. B. B., and Carslaw, K. S.: Quantifying sources of
13 inter-model diversity in the cloud albedo effect, *Geophys. Res. Lett.*, 42, 1568-1575,
14 doi:10.1002/2015GL063301, 2015.
- 15 Yu, H., Chin, M., West, J. J., Atherton, C. S., Bellouin, N., Bergmann, D., Bey, I., Bian, H.,
16 Diehl, T., Forberth, G., Hess, P., Schulz, M., Shindell, D., Takemura, T., and Tan, Q.: A
17 multimodel assessment of the influence of regional anthropogenic emission reductions on
18 aerosol direct radiative forcing and the role of intercontinental transport, *J. Geophys. Res.*,
19 118, 700-720, doi:10.1029/2012JD018148, 2013.
- 20 Zhang, X. Y., Wang, Y. Q., Niu, T., Zhang, X. C., Gong, S. L., Zhang, Y. M., and Sun, J. Y.:
21 Atmospheric aerosol compositions in China: spatial/temporal variability, chemical signature,
22 regional haze distribution and comparisons with global aerosols, *Atmos. Chem. Phys.*, 12,
23 779-799, doi:10.5194/acp-12-779-2012, 2012.



	HadGEM3-GA4			GISS-E2			CESM1		
	Con	Ch0	Ch0-Con	Con	Ch0	Ch0-Con	Con	Ch0	Ch0-Con
Total SO2 (Tg)	0.6370	0.5917	-0.0453	1.1511	1.0753	-0.0758	-	-	-
Total SO4 (Tg)	1.5689	1.4993	-0.0696	1.0907	1.0142	-0.0765	1.4594	1.3234	-0.1360
Mean AOD	0.21692	0.21272	-0.00420	0.13122	0.13090	-0.00032	0.12336	0.12208	-0.00128
Mean TOA SW (W m⁻²)	242.274	242.553	0.279	241.030	240.996	-0.034	236.678	236.864	0.186
Mean temp (K)	289.677	289.791	0.114	288.987	288.959	-0.028	288.047	288.102	0.054
Δ AOD/Δ SO4 (Tg⁻¹)			0.0603			0.00418			0.00941
Δ TOA SW/Δ AOD (W m⁻²)			-66.443			(+)-105.723			-144.961
Total SO4 (Tg)	0.050229	0.015419	-0.034810	0.042600	0.026605	-0.015995	0.054137	0.015172	-0.038965
Mean AOD	0.57565	0.28904	-0.28661	0.23156	0.18459	-0.04697	0.22705	0.15071	-0.07634
Mean TOA SW (W m⁻²)	228.828	234.171	5.343	233.319	234.224	0.905	224.160	228.355	4.195
Mean temp (K)	288.687	289.095	0.407	288.965	289.014	0.049	289.110	289.404	0.294
Δ AOD/Δ SO4 (Tg⁻¹)			8.23			2.94			1.96
Δ TOA SW/Δ AOD (W m⁻²)			-18.642			-19.268			-54.952



- 1 Table 1: Area-integrated SO₂ and SO₄ burdens, area-weighted means of AOD, net down all-
- 2 sky TOA SW flux, and surface temperature, and ratios of mean change in TOA SW to change
- 3 in SO₄ burden and change in AOD, for the globe and the region 100°E - 120°E, 20°N - 40°N.
- 4 Values are shown for each model for the control simulation (Con), the simulation with no SO₂
- 5 emissions from China (Ch0), and the difference (Ch0 – Con). AOD is diagnosed for clear-
- 6 sky conditions in HadGEM3-GA4 and GISS-E2, and for all-sky conditions in CESM1.
- 7 Global SO₂ burden was calculated only for HadGEM3-GA4 and GISS-E2.

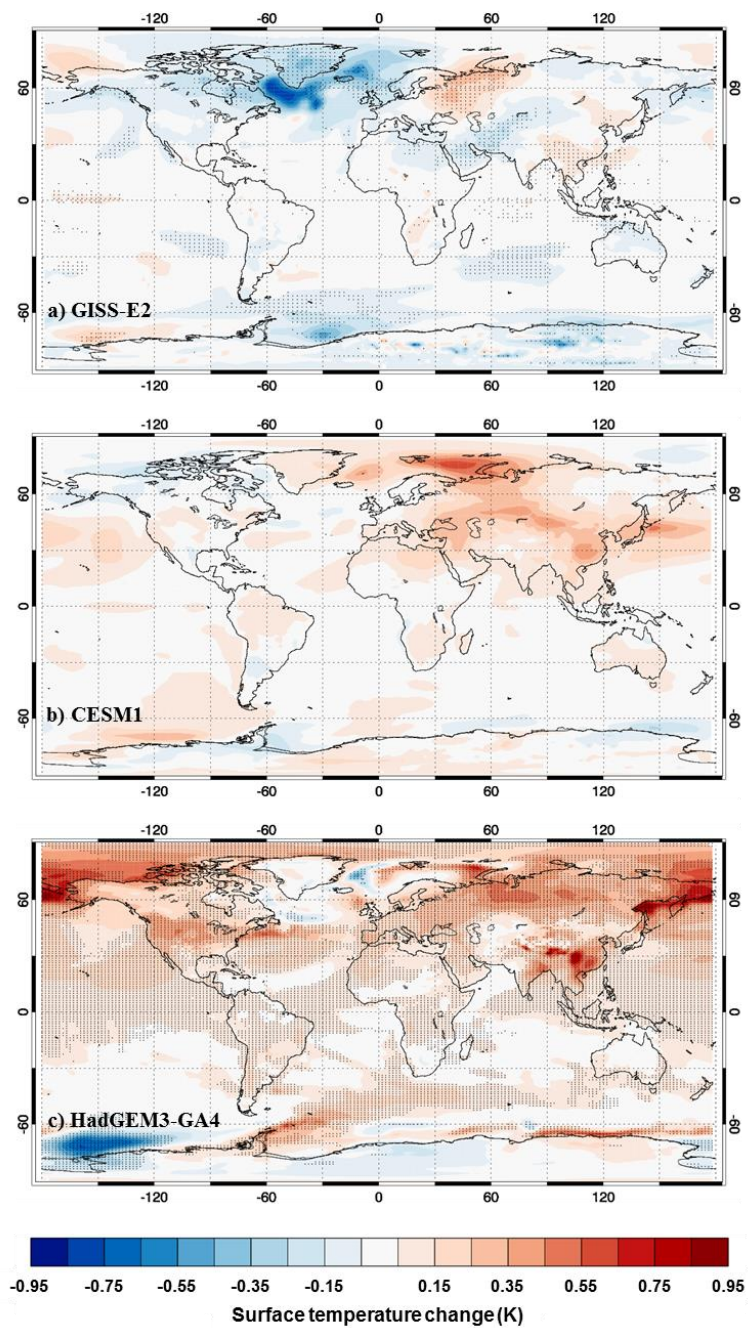


1

2 Figure 1: Change in net down TOA SW flux due to removal of SO₂ emissions over China for
3 a) GISS-E2, b) CESM1, and c) HadGEM3-GA4. Differences are calculated as the 150-year



- 1 mean of the perturbation simulation minus the 150-year mean of the control. Plots focuses on
- 2 the Asian region as changes outside this domain were minimal. Stippling for GISS-E2 and
- 3 HadGEM3-GA4 indicates the change in that grid-box exceeded 2 standard deviations.
- 4 Significance was not evaluated for CESM1 as multiple 150-year control runs were not
- 5 available to assess internal variability for this model.

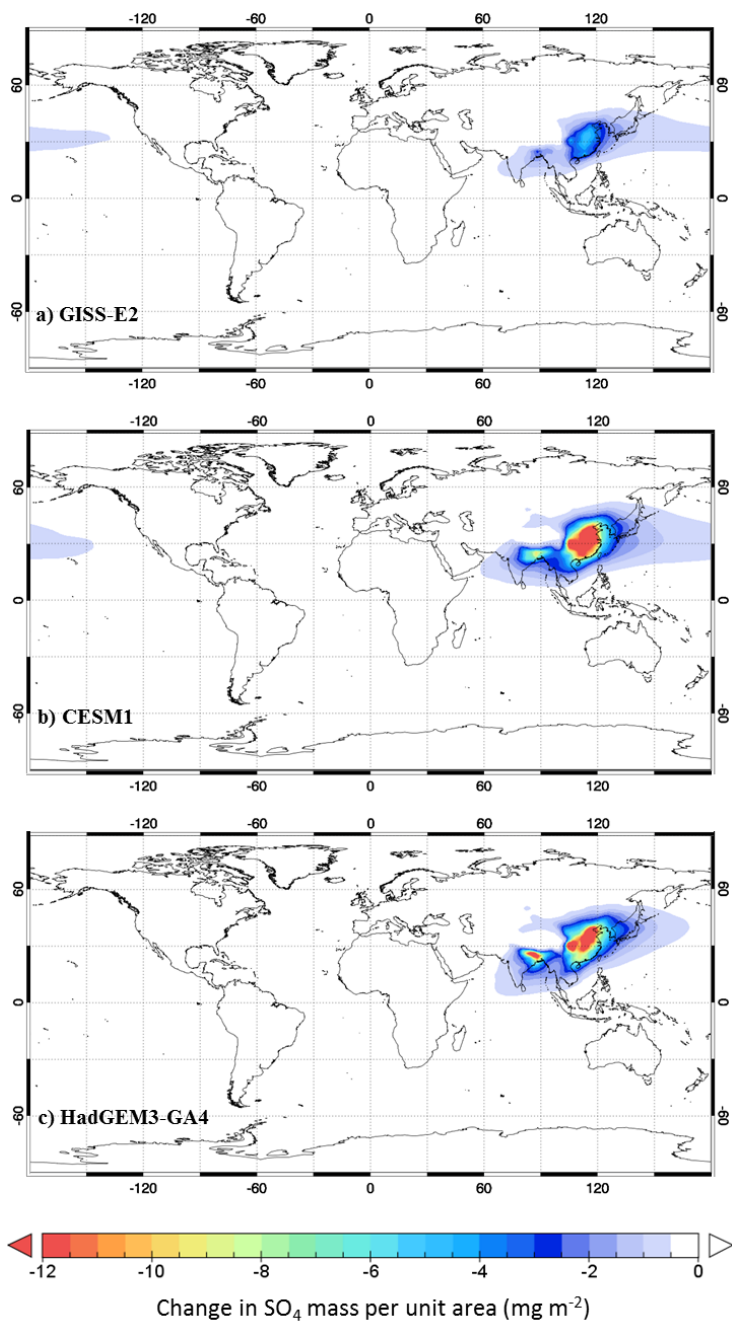


1

2 Figure 2: Global changes in surface temperature due to removing SO₂ emissions from China
3 for a) GISS-E2, b) CESM1, and c) HadGEM3. Differences are for 150-year means of

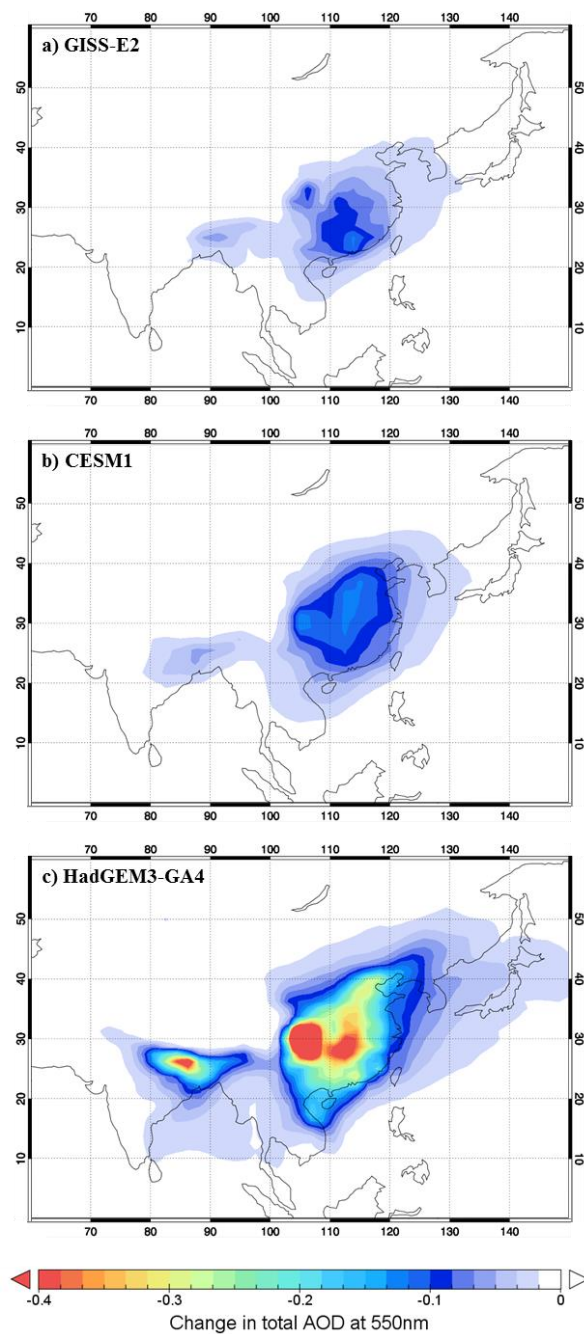


- 1 perturbation simulation minus control simulation. Stippling for GISS-E2 and HadGEM3-
- 2 GA4 indicates changes exceeded two standard deviations for that grid box.



1

2 Figure 3: Global changes in column-integrated SO₄ burden due to removing SO₂ emissions
3 from China, for a) GISS-E2, b) CESM1, and c) HadGEM3-GA4. Differences are calculated
4 as perturbation run minus control run, averaged over 150 years.



1

2 Figure 4: Change in AOD at 550nm due to removing SO₂ emissions from China for a) GISS-
3 E2, b) CESM1, and c) HadGEM3-GA4. For HadGEM3-GA4 and GISS-E2, AOD is
4 calculated for clear-sky conditions, whereas for CESM1 AOD is calculated for all-sky



- 1 conditions, which will generally result in higher values within each simulation. Differences
- 2 are calculated as perturbation run minus control run, averaged over 150 years. The plot
- 3 region focuses on Asia as changes outside of this domain were minimal.